



Check for updates



# Analysis of Interfacial Losses and Passivation Strategies for Narrow-Bandgap Perovskite Solar Cells

<sup>1</sup>Molecular Materials and Nanosystems and Institute for Complex Molecular Systems, Eindhoven University of Technology, Eindhoven, The Netherlands | <sup>2</sup>TNO, Eindhoven, The Netherlands | <sup>3</sup>Dutch Institute for Fundamental Energy Research, AJ Eindhoven, The Netherlands

Correspondence: René A. J. Janssen (r.a.j.janssen@tue.nl)

Received: 14 April 2025 | Revised: 16 June 2025 | Accepted: 16 June 2025

Funding: Netherlands Organization for Scientific Research, Grant/Award Number: NWO Spinoza grant; European Union's Horizon Europe Research and Innovation Programme, Grant/Award Numbers: 101075605, SuPerTandem 101098168, PERSTACK

Keywords: absolute photoluminescence | metal-halide perovskite | narrow bandgap | passivation | quasi-Fermi level splitting

### ABSTRACT

Tin-lead (Sn-Pb) halide perovskites hold promise as narrow-bandgap semiconductors in future solar cells. Currently, non-radiative recombination induced open-circuit voltage losses limit their full potential. To determine their origin, intrinsic and interfacial non-radiative recombination losses are investigated for Sn-Pb perovskite solar cells, and the effects of bulk and surface passivation strategies are assessed. Absolute photoluminescence is used to determine the quasi-Fermi level splitting in perovskite layers, with and without charge transport layers, and distinguish bulk and interface contributions. The intrinsic losses in the perovskite semi-conductor and at its interfaces with the poly(3,4-ethylenedioxythiophene):poly(styrene sulfonate) (PEDOT:PSS) and  $C_{60}$  charge transport layers contribute significantly to the overall voltage deficit. Incorporating glycine hydrochloride as bulk additive during processing reduces the non-radiative losses in the absorber. Likewise, surface passivation with alkane-diammonium iodides or cadmium iodide mitigates the non-radiative recombination induced by the  $C_{60}$  electron transport layer by eliminating direct contact with the perovskite semiconductor. While each of these passivation strategies are beneficial, shortcomings remain in implementing them in actual devices because effective passivation of the perovskite can limit the efficient extraction of charges.

## 1 | Introduction

The increasing global demand for renewable energy sources has fueled extensive research efforts to develop efficient and cost-effective solar cells. Metal halide perovskite solar cells (PSCs) are emerging as a disruptive photovoltaic technology, promising high power conversion efficiency (PCE) and low fabrication costs. The combination of the excellent optoelectronic properties of metal halide perovskites, efficient charge generation, and bandgap tunability underlie the motivation for extensive research [1–3]. For metal halide perovskites with a nominal ABX<sub>3</sub> composition, wide-bandgap absorbers are typically obtained by mixing Br<sup>-</sup> or Cl<sup>-</sup> with I<sup>-</sup> at the X-site, whereas a

narrow bandgap is achieved by alloying  $Pb^{2+}$  with  $Sn^{2+}$  at the B-site [4–8]. These strategies allow tuning the bandgap energy ( $E_g$ ) between 1.2 and 3.0 eV and combined enable the application of metal halide perovskites in multi-junction solar cells [9, 10].

The narrowest bandgaps are obtained with tin–lead (Sn–Pb) perovskites, in which Pb $^{2+}$  and Sn $^{2+}$  ions are present in approximately equal amounts [11–14]. Presently, optimized Sn–Pb PSCs reach PCEs above 23.5% [15–17]. Despite impressive developments, the introduction of Sn $^{2+}$  in the perovskite lattice adversely affects device stability due to the easy oxidation of Sn $^{2+}$ to Sn $^{4+}$ , which leads to high-level p-type doping, short charge carrier lifetimes, and degradation of device performance [13].

This is an open access article under the terms of the Creative Commons Attribution License, which permits use, distribution and reproduction in any medium, provided the original work is properly cited.

© 2025 The Author(s). Solar RRL published by Wiley-VCH GmbH.

This process readily occurs through reactions with the solvent or traces of oxygen [18, 19]. Many approaches have been developed to prevent the oxidation of tin-based perovskites during device fabrication and operation, of which tin fluoride (SnF<sub>2</sub>) is the most commonly employed and elaborately studied reducing agent [20–22].

Beside the oxidation of tin-based perovskites, non-radiative recombination pathways also significantly decrease the performance, by reducing the charge carrier lifetime, the open-circuit voltage ( $V_{\rm OC}$ ), and PCE [23–27]. Non-radiative recombination is associated with defects or trap states in the perovskite and at its interfaces with the charge transport layers (CTLs). Several passivation techniques have been employed to improve the performance of Sn–Pb PSCs, among others, using quasi-two-dimensional perovskites, organic ammonium salts, or cadmium iodide [15, 28–31]. To design effective strategies that suppress or eliminate non-radiative recombination in Sn–Pb PSCs, a detailed understanding of the non-radiative recombination processes and passivation mechanisms is crucial.

Advanced characterization techniques, including time-resolved photoluminescence (PL) spectroscopy and transient absorption spectroscopy, have provided valuable insights into the kinetics and dynamics of non-radiative recombination in Sn-Pb PSCs [32–34]. To identify the origin of the non-radiative losses that reduce the  $V_{\rm OC}$ , one can measure the quasi-Fermi level splitting (QFLS). The QFLS is the difference in the Fermi energies of holes and electrons under nonequilibrium conditions, for example, created by light, and conveniently,  $qV_{\rm OC}$  equals the QFLS under illumination at open circuit [35]. The QFLS can be measured with absolute PL measurements and represents a powerful technique to quantify the contributions of the defects in the perovskite film and at the interfaces between the perovskite and CTLs to the non-radiative recombination losses.

In this work, the effect of passivation strategies on the non-radiative recombination of charge carriers in Sn-Pb PSCs is examined. We begin by analyzing the voltage loss for p-i-n devices and by describing the passivation of bulk and surface defects at the interface of the perovskite with the electron transport layer (ETL) and hole transport layer (HTL). To further understand the working principle of the passivation strategies, we perform light-intensity dependent absolute PL spectroscopy for different HTL and ETL interfaces. We demonstrate that non-radiative recombination occurs in the bulk and at the HTL and ETL interfaces. Additionally, we show that it can be reduced by employing additives to the precursor solution to improve the bulk perovskite and using surface passivation at the perovskite-ETL interface. We also show that while these passivation strategies work well to increase the QFLS, the actual photovoltaic performance of the perfectly passivated perovskite can be compromised by losses that occur when charge extraction is hindered.

## 2 | Results and Discussion

Single-junction PSCs (Figure 1a) were fabricated in an inverted (p-i-n) architecture, with poly (3,4-ethylenedioxythiophene):

poly(styrene sulfonate) (PEDOT:PSS) and  $C_{60}$  serving as the HTL and ETL, respectively. The active layer consists of mixed Sn–Pb iodide perovskite containing cesium, methylammonium (MA), and formamidinium (FA) A-site cations with a nominal  $Cs_{0.1}FA_{0.6}MA_{0.3}Pb_{0.5}Sn_{0.5}I_3$  composition. The perovskite layers were deposited from a 1.8 M precursor solution, in N,N-dimethylformamide/dimethyl sulfoxide 3:1 (v/v). To prevent tin oxidation, tin fluoride (SnF<sub>2</sub>) was added to the precursor solution [21, 36–38]. Further, guanidinium thiocyanate (GuaSCN) salt was added to enhance the stability and morphology of the perovskite film, leading to improved device performance [39, 40]. Detailed information on the fabrication processes and methods is provided in the Supporting Information.

Figure 1b shows the current–density versus voltage (J-V) characteristics in forward and reverse scans of a PSC fabricated without passivation under simulated AM 1.5G illumination calibrated to  $100\,\mathrm{mW}\,\mathrm{cm}^{-2}$ . The device yields a  $V_\mathrm{OC}$  of 750 mV, a short-circuit current density  $(J_\mathrm{SC})$  of 27.5 mA cm<sup>-2</sup>, and a fill factor (FF) of 0.70, leading to a PCE of 14.6%. The external quantum efficiency (EQE) approaches 85% under 1-sun equivalent bias illumination (Figure S1, Supporting Information). The  $J_\mathrm{SC}$  calculated from integrating the product of the EQE and the AM 1.5G spectral irradiance at 1-sun solar intensity reaches 29.3 mA cm<sup>-2</sup>. The device parameters are summarized in Table S1, Supporting Information and Figure S2 shows the boxplots of the device statistics.

The radiative detailed balance limit (DBL) of the  $V_{\rm OC}$  for the Sn-Pb perovskite ( $E_g = 1.27 \,\text{eV}$ , derived from derivative of EQE) is 1000 mV [9]. Hence, the  $V_{\rm OC}$  of the non-passivated PSC lacks a significant 240 mV due to additional losses. These losses mostly result from non-radiative recombination of electrons and holes, which occurs at defects in the bulk, at grain boundaries, and interfaces [41, 42]. To quantify the free energy losses in the bulk and at the interfaces, absolute PL measurements on neat perovskite films or perovskite-CTL combinations were performed from which the QFLS can be determined directly [43-45]. Figure 1c shows the absolute PL spectra of a neat perovskite film on glass (i), and of three (partial) stacks p-i (glass | ITO | PEDOT:PSS | perovskite), i-n (glass | perovskite | C<sub>60</sub>), and p-i-n (glass | ITO | PEDOT: PSS | perovskite |  $C_{60}$ ). The decrease in PL intensity when the HTL, ETL, or both are in contact with the perovskite indicates significant interfacial non-radiative recombination. This is also reflected in the values for the QFLS of each layer combination (Figure 1d).

The QFLS of the neat perovskite film on glass (873 meV) is significantly less than the radiative limit (1000 mV) and indicates substantial non-radiative recombination in the bulk. On top of PEDOT:PSS the QFLS of the perovskite reduces to 800 mV, implying that the HTL-perovskite interface increases the rate of non-radiative recombination by more than one order of magnitude compared to the bulk. Application of  $C_{60}$  on the neat perovskite film, results in a QFLS of 763 meV. The 110 meV loss compared to the QFLS of the neat film implies a close to 70-fold increased non-radiative recombination. For the full p–i–n stack, the QFLS is further reduced to 740 mV and similar to the average  $V_{\rm OC}$  (blue square in Figure 1d). This analysis shows that it is imperative to reduce the recombination losses in the bulk and at the HTL-perovskite and perovskite–ETL interfaces to improve

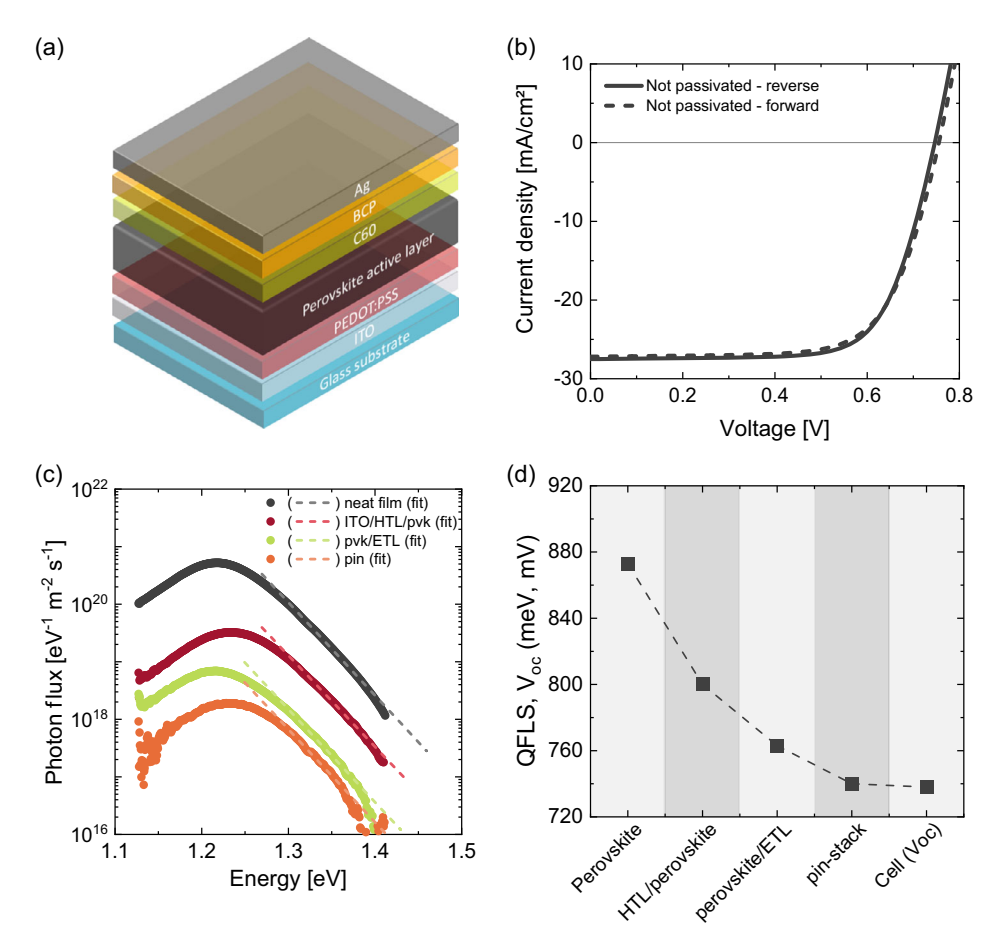


**FIGURE 1** | (a) Layer stack of the ITO | PEDOT:PSS |  $Cs_{0.1}FA_{0.6}MA_{0.3}Pb_{0.5}Sn_{0.5}I_3$  |  $C_{60}$  | BCP | Ag p-i-n device architecture used in this work. (b) J–V measurements in reverse (solid line) and forward (dashed line) scan directions (0.25 V s<sup>-1</sup> with steps of 0.01 V) under simulated AM 1.5G illumination calibrated to 100 mW cm<sup>-2</sup>. (c) Absolute PL spectra (symbols) of different layer stacks with fits (dashed lines) to determine the QFLS. (d) QFLS of neat perovskite films (i) and different layer combinations (p-i, i-n, and p-i-n) and  $V_{OC}$  of the PSC. Note that the  $V_{OC}$  in panels b and d differ due to statistical variations between cells (Figure S2). In panel (d) the average value over 8 cells is plotted.

the  $V_{\rm OC}$ . Different surface passivation strategies have been employed to reduce these losses. Modification of the top and bottom perovskite surfaces with ethane-1,2-diammonium iodide (EDAI<sub>2</sub>) and glycine hydrochloride (GlyHCl), respectively, has been beneficial for mixed Sn-Pb PSCs [15].

The effects of these two passivation strategies were examined in more detail via absolute PL measurements. Figure 2a presents the QFLS of the neat perovskite layer on a glass substrate, without and with EDAI2 and GlyHCl passivation, along with the losses relative to the DBL. The QFLS of the non-passivated films measured  $879 \pm 9$  meV. For perovskite films treated with EDAI<sub>2</sub>  $(0.5 \text{ mg mL}^{-1})$  at the top surface, the QFLS was  $883 \pm 8 \text{ meV}$ , very similar to that of the non-passivated perovskite. By introducing GlvHCl (2 mol%) into the precursor solution, the QFLS of the neat film increased to  $901 \pm 8$  meV. A similar result  $(898 \pm 10 \text{ meV})$  was obtained when both EDAI<sub>2</sub> and GlyHCl were applied. These results indicate that EDAI2 does not reduce the non-radiative losses or improve the bulk or the top surface of the perovskite film. GlyHCl, on the contrary, reduces the nonradiative losses suffered in the neat perovskite absorber layer. If it does not affect the bulk, the successful use of EDAI2 in enhancing the PCE of Sn-Pb PSCs [15] must then be related to improve the interface with the CTLs. Figure 2b depicts the

quantified energy losses in specific layers through a comparison of the QFLS without and with EDAI $_2$  passivation on top and/or GlyHCl passivation incorporated in the bulk. The red bar represents the  $V_{\rm OC}$  of the corresponding PSCs under operation while the other bars correspond to the QFLS of the i, p-i, i-n, and p-i-n stacks and the DBL (Figure S3). The device parameters are summarized in Table S1 and Figure S2 shows the statistics in boxplots.

Figure 2b shows that  $\mathrm{EDAI}_2$  top passivation alone does not improve QFLS of the perovskite on glass (i) or on PEDOT:PSS (p–i), but does reduce the non-radiative recombination in the i–n and p–i–n configurations in which  $\mathrm{C}_{60}$  is on top of the perovskite. With  $\mathrm{EDAI}_2$  between the perovskite and  $\mathrm{C}_{60}$  layer, there is a gain in QFLS of 30 meV for the i–n stack and of 32 meV for the p–i–n stack. This implies that  $\mathrm{EDAI}_2$  passivates the non-radiative recombination occurring at the perovskite- $\mathrm{C}_{60}$  interface. The  $V_{\mathrm{OC}}$  of the PSC with  $\mathrm{EDAI}_2$ , however, only improved by 10 mV to reach 750 mV, which is less than the 774 meV QFLS of the p–i–n stack. The origin of the mismatch between QFLS and  $V_{\mathrm{OC}}$  has been discussed in detail recently and is expected to occur when the diffusion of carriers to the metal contact or CTL is slow compared to the non-radiative recombination in the interface region [46].

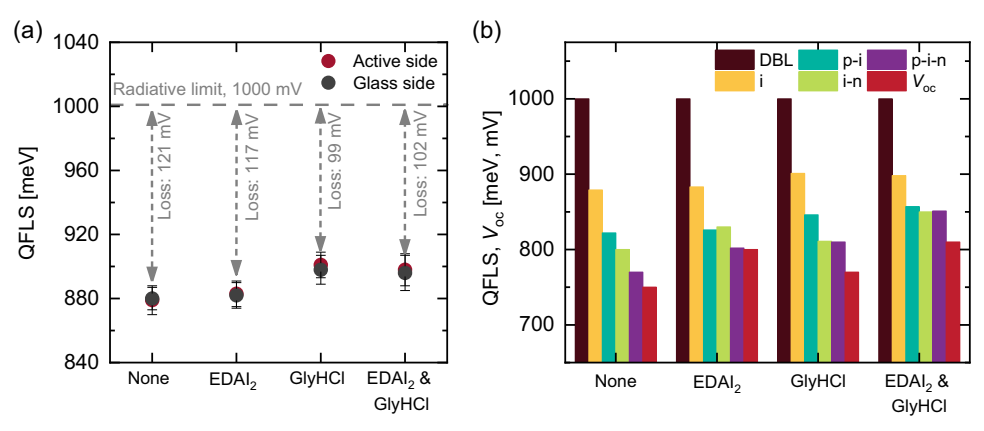


**FIGURE 2** | (a) The QFLS of neat Sn–Pb perovskite films on glass without and with passivation on top and/or incorporated in the bulk and the losses with respect to the radiative limit (DBL) for a 1.27 eV bandgap semiconductor. Measurements were done by exciting and recording from the glass or active layer side. (b) QFLS of neat perovskite films (i) and different layer combinations (p–i, i–n, and p–i–n) and the  $V_{\rm OC}$  of the PSC, for configurations with and without passivation on top and/or incorporated in the bulk, compared to the DBL.

Compared to the non-passivated perovskite, GlyHCl improves both the neat perovskite film (QFLS increase 22 meV) and the perovskite–CTL interfaces (QFLS increase 20 meV for p–i, 11 meV for i–n, and 40 meV for p–i–n) (Figure 2b). These improvements are primarily attributed to higher quality perovskite film formation assisted by the GlyHCl additive. GlyHCl is known to ameliorate the quality and morphology of the perovskite [15, 47]. These observations align with previous studies where GlyHCl additives led to the accumulation of GlyH<sup>+</sup> cations within the lower portion of the perovskite layer, alongside an enhancement in film crystallinity [15]. Additionally, in our previous study we delved deeper into the effect and concentration dependency of the GlyHCl additive for this perovskite composition [48]. Nevertheless, despite the improved crystallization, losses at the perovskite–CTL interfaces remain considerable.

When both passivation techniques are combined, it can again be seen that EDAI $_2$  selectively improves the perovskite–ETL interface. Compared to GlyHCl passivation alone, the QFLSs of the i and p–i stacks are not changed by EDAI $_2$ , but the i–n and p–i–n stacks gain 39 and 41 meV, respectively. While the  $V_{\rm OC}$  improves to 810 mV, it is less than the QFLS of the p–i–n stack (851 meV). Hence, while EDAI $_2$  improves the QFLS of p–i–n stacks considerably without and with using GlyHCl, this gain is only partly reflected in the increase in  $V_{\rm OC}$ . Additionally, the  $J\!-\!V$  characteristics exhibited more pronounced hysteresis in these devices. This minimal improvement may be attributed to the concentration used, suggesting that an optimized concentration could be necessary for further enhancements.

Summarizing, surface passivation by  $EDAI_2$  revealed notable effects on the perovskite–ETL interface, while GlyHCl diminishes both the intrinsic losses of the perovskite and those at the interfaces with the CTLs. While both passivation methods are useful for enhancing the PCE, the intrinsic losses and the additional losses at the CTLs necessitate further optimization of bulk and interfaces for further efficiency gains.

To further investigate the effects of the passivation techniques and confirm these results, light intensity-dependent measurements were performed. By measuring the QFLS as a function of the light intensity, the implied efficiency of a neat material can be quantified, only limited by the non-radiative recombination processes taking place in the bulk and at the surfaces in absence of charge transport losses [49, 50]. Figure 3a shows the PL spectra of a neat perovskite film recorded at different illumination intensities ranging from 0.002 to 1.5-sun equivalents. The resulting QFLSs for the neat perovskite film without passivation, with EDAI2 passivation on top, GlyHCl passivation incorporated in the bulk, and a combination of both passivation techniques are shown in Figure 3b as function of the natural logarithm of the number of incident photons. From the slope, the radiative ideality factor  $(n_{\rm ID})$  can be determined. The corresponding values are summarized in Table 1. The  $n_{\rm ID}$  is sensitive to the mechanism of charge recombination, but its detailed interpretation is hampered by the fact that values close to 1 are expected for both band-to-band and surface recombination, while values closer to 2 are expected for trap-assisted recombination [51].

For the neat perovskite film,  $n_{\rm ID}$  was 1.38. The EDAI $_2$  passivated perovskite shows a very similar  $n_{\rm ID}$  of 1.31, confirming the result from the QFLS measurements that EDAI $_2$  does not significantly affect the neat perovskite. Upon introducing GlyHCl,  $n_{\rm ID}$  slightly reduces to 1.23. When the quantum yield is relatively low, particularly when comparing different stacks with similar QFLS, the  $n_{\rm ID}$  remains unaffected by bimolecular recombination, as its contribution is minimal compared to Shockley–Read–Hall (SRH) recombination. The decrease in  $n_{\rm ID}$  observed with GlyHCl suggests a reduction in bulk recombination, indicating a shift toward surface recombination limitation. This aligns with expectations, as GlyHCl was incorporated into the perovskite bulk and influenced crystallinity [52, 53].

The QFLS under illumination represents the internal voltage multiplied by the elementary charge q, and considering the illumination being directly proportional to the generated photocurrent, one can convert the QFLS-intensity characteristics to pseudo J–V characteristics [49]. The QFLS at 1 sun equivalent light intensity equals the implied or pseudo open-circuit voltage (pV<sub>OC</sub>). The pseudo short-circuit current density (pJ<sub>SC</sub>) (30 mA cm<sup>-2</sup>) has been estimated from the bandgap of the perovskite assuming an EQE of 90%. Then, one can derive the pseudo

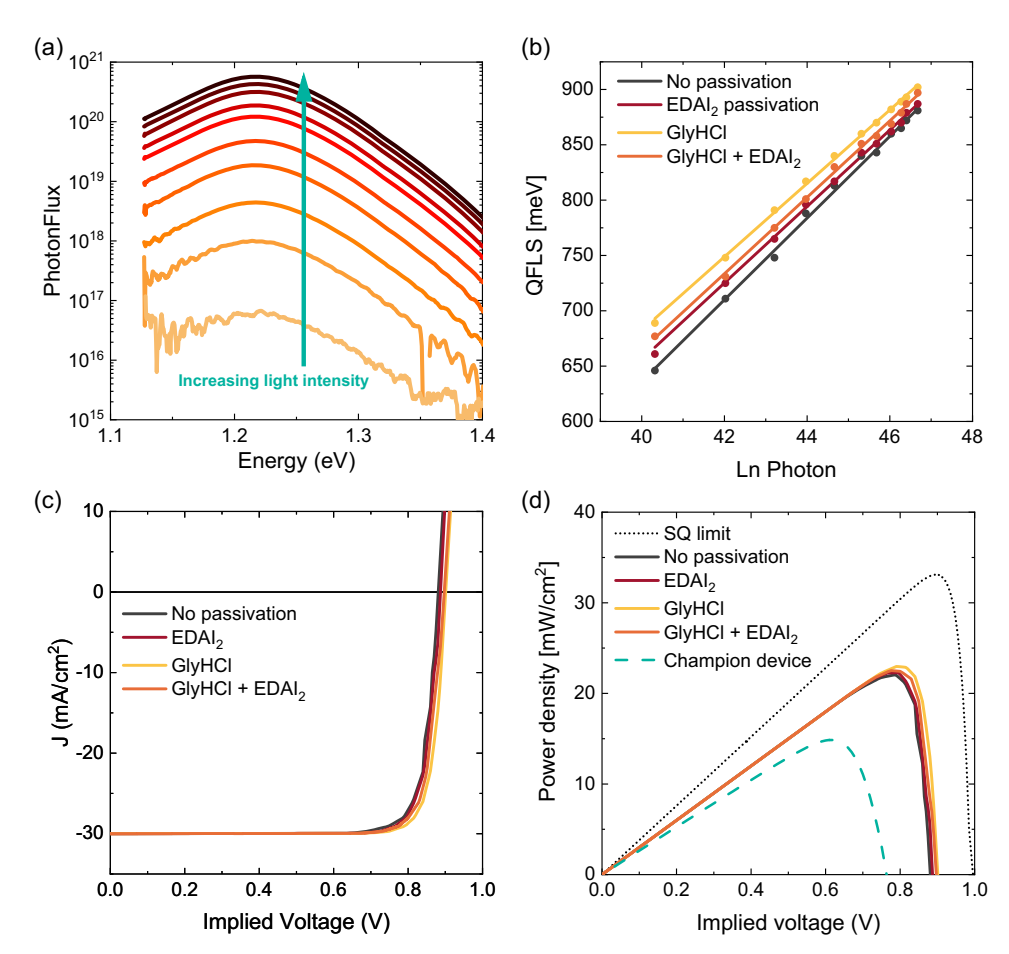


**FIGURE 3** I (a) Absolute PL spectra at various illumination intensities for a neat Sn-Pb perovskite film on glass without passivation. (b) QFLS as a function of natural logarithm of the number of incident photons for a neat perovskite film on glass, without passivation (red circles), with EDAI $_2$  surface passivation (yellow circles), and with GlyHCl bulk passivation (orange circles). (c) Pseudo J-V characteristics for neat perovskite films on glass, without passivation (red line), with EDAI $_2$  surface passivation (yellow line), and GlyHCl bulk passivation (orange line). (d) Pseudo power density characteristics for neat perovskite films on glass, without passivation, with EDAI $_2$  surface passivation and GlyHCl bulk passivation. The corresponding curves for the DBL for a 1.27 eV bandgap material and that of a typical PSC with the same passivation are also shown.

FF (pFF) and the pseudo PCE (pPCE), which provides the implied efficiency of the configuration when there would be no transport losses. The pseudo J-V characteristics of a neat perovskite film on glass without and with passivation by EDAI2 or GlyHCl, reconstructed from the light intensity dependent QFLS, are shown in Figure 3c. The corresponding pseudo power density characteristics are shown in Figure 3d and the respective implied photovoltaic performance parameters are summarized in Table 1. The pseudo J-V characteristics of non-passivated and EDAI2 top-passivated neat perovskite films are virtually identical. However, using GlyHCl passivation improved the pseudo J-V characteristics and pPCE. This improvement is reflected in a higher pFF for the neat films passivated with GlyHCl, whereas the EDAI<sub>2</sub> top passivation has no effect on the pFF compared to the non-passivated film. The increase in pFF for the GlyHCl-passivated film is accompanied by a decrease in the  $n_{\rm ID}$ , reflecting an inverse relationship commonly observed in such cases [49].

The outcome from Figure 2b that  $EDAI_2$  passivates the Sn-Pb perovskite- $C_{60}$  interface, concurs with a previous result that in wide-bandgap perovskite p-i-n devices sub-bandgap defects are situated in proximity of the perovskite-fullerene interface

[25, 26]. Previous studies have shown that also surface treatment with cadmium iodide ( $\mathrm{CdI}_2$ ) results in significantly enhanced efficiency and stability of PSCs [54]. Another alternative proven to enhance performance is propane-1,3-diammonium iodide (PDAI<sub>2</sub>) [55, 56]. Therefore, we will investigate these passivation techniques in greater detail for the narrow bandgap PSCs to further understand their effect.

To understand the interface passivation in more detail, the concentrations of  $EDAI_2$ ,  $PDAI_2$ , and  $CdI_2$  were systematically varied in the range between 0 and 1 mg mL<sup>-1</sup>, and the QFLS for glass | perovskite |  $C_{60}$  (i–n) stacks was examined using absolute PL measurements (Figure 4). The QFLS for all relevant stack configurations (i, p–i, i–n, and p–i–n) can be found in Figure S4. The QFLS of the neat perovskite layer on glass is independent of increasing the thickness of the  $EDAI_2$ ,  $PDAI_2$ , or  $CdI_2$  passivation layer by using more concentrated solutions (gray bars in Figure 4). Although surface molecules may influence the electronic structure of the perovskite surface and contribute to defect passivation [30], we observe that the QFLS remains essentially unchanged when comparing the neat perovskite films with or without top passivation. This suggests that the surface treatments used in this work do not significantly alter the electronic

**TABLE 1** Implied photovoltaic parameters obtained from the pseudo J–V characteristics of neat perovskite films with different passivation and the ideality factor (nID) from QFLS. The prefix "p" indicates values derived from pseudo *J–V* curves rather than standard *J–V* measurements.

	$n_{ m ID}$	pFF (%)	$pV_{OC}$ (V)	$pJ_{SC}$ (mA cm <sup>-2</sup> )	pPCE (%)
No passivation	1.38	$83.3 \pm 0.1$	$0.87 \pm 0.01$	30.0	$22.2 \pm 0.3$
$EDAI_2$	1.31	$83.7 \pm 0.1$	$0.88 \pm 0.01$	30.0	$22.3 \pm 0.4$
GlyHCl	1.23	$85.0 \pm 0.1$	$0.90 \pm 0.01$	30.0	$22.9 \pm 0.3$
$GlyHCl + EDAI_2$	1.28	$84.2 \pm 0.1$	$0.89 \pm 0.01$	30.0	$22.5 \pm 0.3$

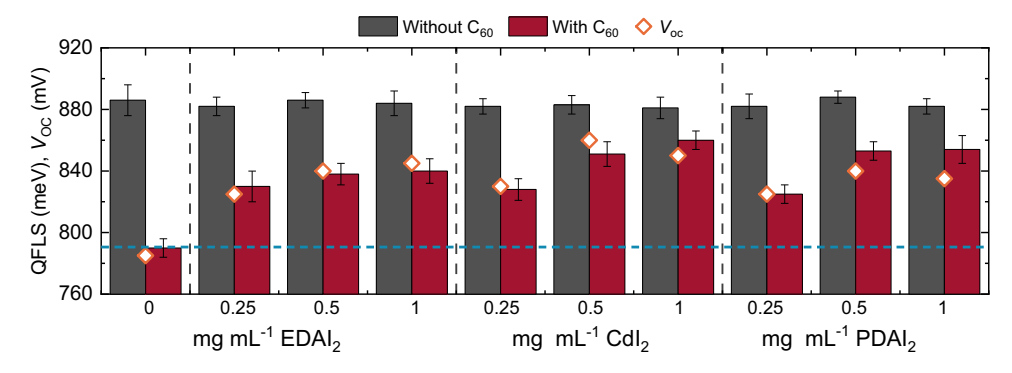


**FIGURE 4** | QFLS at 1-sun equivalent illumination conditions for different surface passivation agents (EDAI<sub>2</sub>, CdI<sub>2</sub>, and PDAI<sub>2</sub>) of neat Sn-Pb perovskite films on glass without and with  $C_{60}$  on top as function of the concentration of the passivating agent in the solution. The  $V_{OC}$  of the corresponding PCSs is also shown. The dashed blue line indicates the QFLS of the Sn-Pb perovskite with  $C_{60}$  on top without passivation.

structure at the surface, or at least not in a way that impacts the optoelectronic quality of the film.

In contrast to the unchanged QFLS of neat perovskite film, the QFLS of the perovskite films with  $C_{60}$  on top increases when using an increased concentration (and thus thickness) for all three passivation agents (red bars in Figure 4). Likewise, the  $V_{\rm OC}$  increases with concentration, but only to a certain limit, beyond which it decreases again (open diamonds in Figure 4). Other photovoltaic performance parameters remained constant but started to deteriorate at the highest concentrations used (Figures S5–S7) and, hence, we did not increase the concentration of the passivation layer over a wider range.

These results imply that the enhanced non-radiative recombination at the perovskite-C<sub>60</sub> interface can be mitigated to a considerable extent by each of the three passivating agents. The fact the OFLS increases for thicker passivation layers suggests that the passivating effect is not due to an improved energy level alignment. Instead, passivation involves eliminating the direct contact between the perovskite semiconductor and C<sub>60</sub>. The  $V_{\rm OC}$  enhances proportionally to the reduction of non-radiative recombination until the passivating layer reaches a critical thickness threshold, at which point the interlayer starts to hinder carrier transport, as also observed in previous our work on a range of triple-cation mixed halide wide-bandgap perovskites [57]. In that study, we applied lithium fluoride (LiF) and choline chloride as top passivation layers and noted similar trends, including: (i) negligible differences between neat perovskite layers with and without top passivation, (ii) passivation at the perovskite-ETL interface enhance the QFLS, and (iii) a clear concentration/thickness dependent behavior.

It has been shown that diammonium ions result in n-doping of the surface [58], resulting in reduced carrier recombination at the perovskite– $C_{60}$  interface, which enhances the  $V_{\rm OC}$  [59]. The possibility of n-type doping by EDAI<sub>2</sub> was investigated in detail by Hu et al. [15], who found that the Fermi level shifts marginally (0.02 eV) closer to the conduction band minimum for EDAI<sub>2</sub>-treated films for the perovskite used in this study, when using the GlyHCl additive. The impact of any n-doping by EDAI<sub>2</sub>, CdI<sub>2</sub>, or PDAI<sub>2</sub> appears to be small for the neat perovskite films, because the QFLS remains essentially unchanged for perovskite films with and without top passivation (Figure 4, gray bars). Alternatively, n-type doping of the perovskite layer may improve the energy alignment at the contact, but EDAI<sub>2</sub> enhances the QFLS of the p-i-n stack to a similar extent as the  $V_{\rm OC}$  of the cell (Figure 2b), which does not directly support this possibility.

We consider that thicker passivation layers reduce the likelihood of a defect state occurring between the perovskite defect and the  $C_{60}$  layer, but may induce a barrier for charge transport. This is also supported by transient photovoltage (TPV) measurements on PSCs with the different EDAI<sub>2</sub> concentrations as top passivation (Figure S8). We observed increased rise and decay times for the passivated devices, indicating the slower extraction (increased rise time) and passivation (increased decay times) [60].

In PSCs, passivation of the perovskite– $C_{60}$  interface by  $CdI_2$  provided the highest, consistent PCEs among the three passivation agents tested (Figures S5–S7), with the intermediate concentration of 0.5 mg mL<sup>-1</sup>  $CdI_2$  providing the highest and consistent  $V_{\rm OC}$  and PCE. We assume that at this concentration  $CdI_2$  adequately occupies ionic vacancies on the perovskite film surface while maintaining a sufficiently low coverage to prevent

the formation of an insulating layer between the perovskite and  $C_{60}$ . We note that higher concentrations of  $EDAI_2$  and  $PDAI_2$  led to increased hysteresis phenomena in the J-V characteristics. Consequently, overly thick passivation layers introduce new challenges that require further optimization.

To further improve the performance of PSCs several strategies could be considered. It is not likely that the thin passivation layers are fully closed. Hence, one possible improvement may come from ultrathin fully closed passivation layers that preserve the defect-suppressing function while maintaining good charge transport. Another option is the use of point contacts. For example, Mao et al. used patterned lithium fluoride (LiF) insulator contacts at the perovskite-ETL interface that combine good charge extraction and effective surface passivation [61]. A third option might the design passivation ligands with builtin conductive or dipolar functionality that enhance charge transfer across the interface. Finally, fullerene-based ETLs can possibly be replaced by ETLs that cause less nonradiative recombination. Recently, cyano-functionalized bithiophene imide dimer-based n-type polymers with tuned energy levels and passivating properties have been used successfully for this purpose [62].

Non-radiative recombination in PSCs is generally considered to be a combination of trap-assisted surface (or interface) recombination at the perovskite–CTL interfaces and trap-assisted Shockley–Read–Hall (SRH) recombination in the bulk. In an attempt to elucidate the underlying mechanisms, light intensity-dependent measurements were conducted for EDAI<sub>2</sub>, CdI<sub>2</sub>, and PDAI<sub>2</sub> passivation. Figure S9 gives a complete overview of the light intensity

dependent measurements of all sub-stacks of the p-i-n configuration. For EDAI2 the results of the perovskite | C60 (i-n) stack are shown in Figure 5a. The light intensity dependent data were converted into pseudo J-V characteristics (Figures S10-S12) and are shown for the EDAI2 i-n stack in Figure 5b. The effect of the concentration of the three passivating agents on  $n_{\rm ID}$ , pFF, and pPCE is shown in Figure S13 and summarized for the glass | perovskite | C<sub>60</sub> stacks (i-n) in Figure 5c-e. The data reveal that for all three passivation materials the effect of surface passivation is most significant for i-n and p-i-n stacks. When C<sub>60</sub> is deposited on top of a neat perovskite film, the implied  $V_{\rm OC}$  and pFF drop, accompanied by an increase of  $n_{\rm ID}$ . When passivating the pervskite- $C_{60}$  the implied  $V_{OC}$  and pFF increase, while  $n_{ID}$ decreases concomitantly. Overall, these trends tend to increase with the thickness of the passivation layer. Interpreting the ideality factor in simple terms of a dominant recombination mechanism is difficult. It is thought that interfacial recombination leads to a lower  $n_{\rm ID}$  compared to SRH recombination in the bulk [51], but our results suggest opposite behavior, that is, a reduced interface recombination, and thus a higher implied  $V_{\rm OC}$  and pFF, leads to a lower  $n_{\rm ID}$ .

For the hole-collecting contact, the data reveal that the implied  $V_{\rm OC}$  of the perovskite layer is lowered to average of 860 meV when it is processed on a PEDOT:PSS layer (p-i) instead of on glass (i), which has an implied  $V_{\rm OC}$  of 900 meV. However, no effects of surface passivation of the perovskite with either EDAI<sub>2</sub>, CdI<sub>2</sub>, or PDAI<sub>2</sub> are observed. There is only a minor effect on the implied  $V_{\rm OC}$  or  $n_{\rm ID}$  derived from it (Figures S4, and S10–S12). Overall, the  $n_{\rm ID}$  and pFF are similar for perovskite

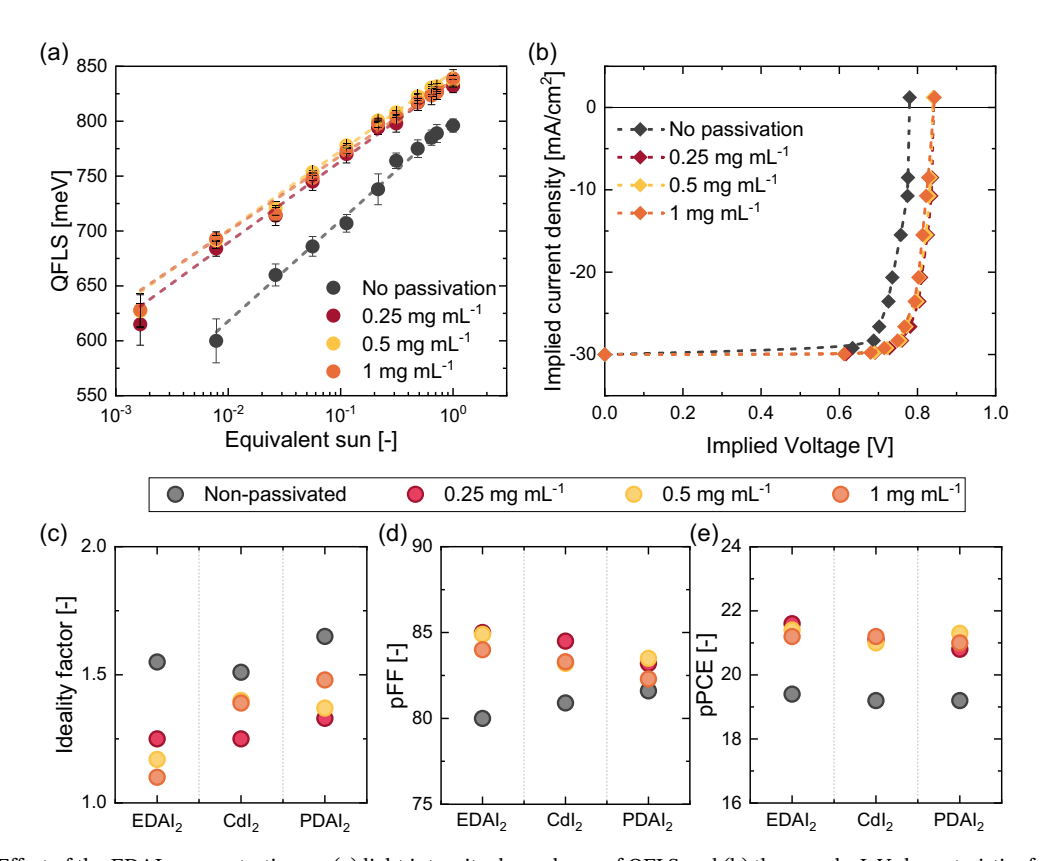


**FIGURE 5** | Effect of the EDAI<sub>2</sub> concentration on (a) light intensity dependency of QFLS and (b) the pseudo J-V characteristics for perovskite |  $C_{60}$  stack. The derived (c)  $n_{\text{ID}}$ , (d) pFF, and (e) pPCE for the glass | perovskite |  $C_{60}$  stacks (i–n) for the different passivation agents and concentrations.

layers on glass and on PEDOT:PSS. Compared to the i stack the pPCE of the p–i stack is primarily reduced because of an unrecoverable loss of implied  $V_{\rm OC}$ .

For all concentrations of surface passivation, the pPCE is most improved for the perovskite |  $C_{60}$  (i–n) and the glass | ITO | PEDOT:PSS | perovskite |  $C_{60}$  (p–i–n) stacks, upon application of surface passivation, as we observe an increase from around 19% to 21%. The layers processed on glass (i) or on ITO | PEDOT:PSS (p–i) show almost no variation in pPCE. However, we note that within the concentration range used, passivation does not recover the implied  $V_{\rm OC}$  or pFF in i–n and p–i–n configurations to the level of the corresponding i and p–i stacks and –as result– the pPCE is reduced from about 22% to 19%–21%. This indicates that improvements still need to be made.

## 3 | Conclusion

We performed a loss analysis using absolute photoluminescence spectroscopy on narrow-bandgap PSCs and identified the nonradiative recombination losses in the bulk of the perovskite, at the interfaces, and at the contacts. The non-radiative recombination of charges in the neat Sn-Pb perovskite semiconductor and its interface with the C<sub>60</sub> charge transport layer introduce a significant loss in the implied  $V_{\rm OC}$ . Incorporation of GlyHCl into the precursor solution reduced the intrinsic non-radiative losses suffered in the neat Sn-Pb perovskite layer and resulted in an improved semiconductor quality. Surface passivation with EDAI2, CdI2, and PDAI2 effectively mitigated the adverse effect of the C<sub>60</sub> ETL. This passivation mainly involves eliminating the direct contact between the perovskite semiconductor and the C<sub>60</sub> layer and can be improved by using thicker passivation layers, albeit ultimately hampering efficient charge extraction. These results highlight the factors limiting the performance of a narrow-bandgap PSC and identify the nature of passivation strategies in terms of bulk and interface effects in reducing non-radiative recombination. While reducing non-radiative recombination increases the QFLS, effective passivation can also limit the efficient extraction of charges and thereby compromise the device efficiency. The use of fully-closed, ultrathin passivation layers or designing ligands with conductive or dipolar functionalities could balance defect passivation with efficient charge transport, and therefore be the next step to take to improve Sn-Pb-based narrow-bandgap PSCs.

## Acknowledgements

The authors thank Guus Aalbers for the TPV measurements. The authors acknowledge funding from the Netherlands Organization for Scientific Research (NWO Spinoza grant). The work of L.M.K. is supported by HyET Solar Netherlands B.V. B.B. acknowledges funding from the European Union's Horizon Europe research and innovation programme (Grant Agreement No. 101075605, SuPerTandem). The project has also received funding from the European Research Council (ERC) under the European Union's Horizon Europe research and innovation programme (Grant Agreement No. 101098168, PERSTACK).

## **Conflicts of Interest**

The authors declare no conflicts of interest.

### **Data Availability Statement**

The data that support the findings of this study are available from the corresponding author upon reasonable request.

#### References

- 1. Y. Zhou, I. Poli, D. Meggiolaro, F. De Angelis, and A. Petrozza, *Nature Reviews Materials* 6 (2021): 986–1002.
- 2. S. D. Stranks and H. J. Snaith, Nature Nanotechnology 10 (2015): 391-402.
- 3. P. K. Nayak, S. Mahesh, H. J. Snaith, and D. Cahen, *Nature Reviews Materials* 4 (2019): 269–285.
- 4. J. Xu, C. C. Boyd, Z. J. Yu, et al., Science 367 (2020): 1097-1104.
- 5. Z. Song, C. Chen, C. Li, R. A. Awni, D. Zhao, and Y. Yan, Semiconductor Science and Technology 34 (2019): 093001.
- 6. A. Kojima, K. Teshima, Y. Shirai, and T. Miyasaka, *Journal of the American Chemical Society* 131 (2009): 6050–6051.
- 7. J. H. Noh, S. H. Im, J. H. Heo, T. N. Mandal, and S. Il Seok, *Nano Letters* 13 (2013): 1764–1769.
- 8. N. Kitazawa, Y. Watanabe, and Y. Nakamura, *Journal of Materials Science* 37 (2002): 3585–3587.
- 9. W. Shockley and H. J. Queisser, Journal of Applied Physics 32 (1961): 510-519.
- 10. F. Meillaud, A. Shah, C. Droz, E. Vallat-Sauvain, and C. Miazza, *Solar Energy Materials and Solar Cells* 90 (2006): 2952–2959.
- 11. J. Wang, K. Datta, J. Li, et al., Advanced Energy Materials 10 (2020): 2000566.
- 12. K. J. Savill, A. M. Ulatowski, and L. M. Herz, *ACS Energy Letters* 6 (2021): 2413–2426.
- 13. W. Ke, C. C. Stoumpos, and M. G. Kanatzidis, *Advanced Materials* 31 (2019): 1803230.
- 14. J. Seo, T. Song, S. Rasool, S. Park, and J. Y. Kim, Advanced Energy and Sustainability Research 4 (2023): 2200160.
- 15. S. Hu, K. Otsuka, R. Murdey, et al., Energy & Environmental Science 15 (2022): 2096–2107.
- 16. R. Lin, Y. Wang, Q. Lu, et al., Nature 620 (2023): 994-1000.
- 17. S. Hu, J. Wang, P. Zhao, et al., Nature 639 (2025): 93-101.
- 18. M. I. Saidaminov, I. Spanopoulos, J. Abed, et al., ACS Energy Letters 5 (2020): 1153–1155.
- 19. J. Pascual, G. Nasti, M. H. Aldamasy, et al., *Materials Advances* 1 (2020): 1066–1070.
- 20. S. Gupta, D. Cahen, and G. Hodes, *Journal of Physical Chemistry C* 122 (2018): 13926–13936.
- 21. K. J. Savill, A. M. Ulatowski, M. D. Farrar, M. B. Johnston, H. J. Snaith, and L. M. Herz, *Advanced Functional Materials* 30 (2020): 2005594.
- 22. J. Zillner, H. Boyen, P. Schulz, et al., *Advanced Functional Materials* 32 (2022): 2109649.
- 23. S. Mahesh, J. M. Ball, R. D. J. Oliver, et al., Energy & Environmental Science 13 (2020): 258–267.
- 24. P. Chen, Y. Bai, and L. Wang, Small Structures 2 (2021): 2000050.
- 25. B. T. van Gorkom, T. P. A. van der Pol, K. Datta, M. M. Wienk, and R. A. J. Janssen, *Nature Communications* 13 (2022): 349.
- 26. J. Warby, F. Zu, S. Zeiske, et al., Advanced Energy Materials 12 (2022): 2103567.
- 27. M. Stolterfoht, C. M. Wolff, J. A. Márquez, et al., *Nature Energy* 3 (2018): 847–854.

- 28. T. Zhu, D. Zheng, J. Liu, L. Coolen, and T. Pauporté, ACS Applied Materials & Interfaces 12 (2020): 37197–37207.
- 29. K. Datta, J. Wang, D. Zhang, et al., *Advanced Materials* 34 (2022): 2110053
- 30. D. Yu, Q. Wei, H. Li, et al., Angewandte Chemie 13 (2022): e202202346.
- 31. T. Jiang, X. Xu, Z. Lan, et al., Nano Energy 101 (2022): 107596.
- 32. S. Narra, E. Jokar, O. Pearce, C. Y. Lin, A. Fathi, and E. W. G. Diau, *Journal of Physical Chemistry Letters* 11 (2020): 5699–5704.
- 33. T. Jiang, Z. Chen, X. Chen, et al., ACS Energy Letters 4 (2019): 1784–1790.
- 34. J. Tong, Z. Song, D. H. Kim, et al., Science 364 (2019): 475-479.
- 35. P. Wurfel, Journal of Physics C: Solid State Physics 15 (1982): 3967.
- 36. S. J. Lee, S. S. Shin, Y. C. Kim, et al., Journal of the American Chemical Society 138 (2016): 3974–3977.
- 37. R. Lin, K. Xiao, Z. Qin, et al., Nature Energy 4 (2019): 864-873.
- 38. T. Nakamura, S. Yakumaru, M. A. Truong, et al., *Nature Communications* 11 (2020): 3008.
- 39. J. Zou, W. Liu, W. Deng, et al., *Electrochimica Acta* 291 (2018): 297–303.
- 40. S. Zhong, Z. Li, C. Zheng, et al., Solar RRL 6 (2022): 2200176.
- 41. B. Chen, P. N. Rudd, S. Yang, Y. Yuan, and J. Huang, *Chemical Society Reviews* 48 (2019): 3842.
- 42. T. S. Sherkar, C. Momblona, L. Gil-Escrig, et al., *ACS Energy Letters* 2 (2017): 1214–1222.
- 43. D. Abou-ras, T. Kirchartz, and U. Rau, Advanced Characterization Techniques for Thin Film Solar Cells (Wiley-VCH Verlag GmbH & Co, 2016).
- 44. T. Kirchartz and U. Rau, *Physica Status Solidi A: Applications and Materials Science* 205 (2008): 2737–2751.
- 45. P. Wurfel and U. Wurfel, Physics of Solar Cells from Basic Principles to Advanced Concepts, 3<sup>rd</sup> ed., (Wiley-VCH Verlag GmbH & Co, 2016).
- 46. J. Warby, S. Shah, J. Thiesbrummel, et al., *Advanced Energy Materials* 13 (2023): 2303135.
- 47. H. Cheng, J. Zhuang, J. Cao, T. Wang, W. Y. Wong, and F. Yan, Journal of Materials Chemistry A 12 (2023): 2151–2156.
- 48. L. M. Kessels, W. H. M. Remmerswaal, L. M. van der Poll, et al., *Solar RRL* 8 (2024): 2400506.
- 49. M. Stolterfoht, M. Grischek, P. Caprioglio, et al., *Advanced Materials* 32 (2020): 2000080.
- 50. M. Grischek, P. Caprioglio, J. Zhang, et al., Solar RRL 6 (2022): 2200690.
- 51. P. Caprioglio, C. M. Wolff, O. J. Sandberg, et al., Advanced Energy Materials 10 (2020): 2000502.
- 52. W. Tress, M. Yavari, K. Domanski, et al., Energy & Environmental Science 11 (2018): 151–165.
- 53. D. Głowienka, D. Zhang, F. Di Giacomo, et al., *Nano Energy* 67 (2020): 104186.
- 54. W. Q. Wu, P. N. Rudd, Z. Ni, et al., *Journal of the American Chemical Society* 142 (2020): 3989–3996.
- 55. C. Liu, Y. Yang, H. Chen, et al., Science 382 (2023): 810-815.
- 56. H. Lee, Y. Kang, S. Kwon, D. Kim, and S. Na, *Small Methods* 8 (2023): 2300948.
- 57. W. H. M. Remmerswaal, B. T. van Gorkom, D. Zhang, M. M. Wienk, and R. A. J. Janssen, *Advanced Energy Materials* 14 (2024): 2303664.

- 58. X. Jiang, Q. Zhou, Y. Lu, et al., National Science Review 11 (2024): nwae0055.
- 59. X. Jiang, F. Wang, Q. Wei, et al., Nature Communications 11 (2020): 1245.
- 60. S. Ravishankar, L. Kruppa, S. Jenatsch, G. Yan, and Y. Wang, *Energy & Environmental Science* 17 (2024): 1229–1243.
- 61. K. Mao, F. Cai, Z. Zhu, et al., Advanced Energy Materials 13 (2023): 2302132.
- 62. K. Feng, G. Wang, Q. Lian, et al., Nature Materials 24 (2025): 770-777.

## **Supporting Information**

Additional supporting information can be found online in the Supporting Information section.